ELSEVIER

International Journal of Mass Spectrometry 204 (2001) 281–294

International Journal of Mass Spectrometry

Sigma bond activation by transition metal ions: the $Co(CH_4)_n^+$ systems revisited

Qiang Zhang, Paul R. Kemper, Seung Koo Shin[1], Michael T. Bowers*

Department of Chemistry, University of California, Santa Barbara, California 93106-9510, USA

Received 18 May 2000; accepted 20 July 2000

Abstract

Measurements are reported for sequential clustering of CH_4 to Co^+ ions under equilibrium conditions. The CH_4 cluster bond strengths show a pairwise behavior: $-\Delta H_0^0 = 23.1$ and 25.3 kcal/mol for $n = 1$ and 2; 7.3 and 5.2 kcal/mol for $n = 3$ and 4; and ~2 kcal/mol for both $n = 5$ and 6. This pairwise behavior is well reproduced by large basis set density functional theory calculations. These calculations indicate $n = 1$ and $n = 2$ add on opposite sides of the Co^+ ion in η^2 configuration and induce significant *s/d* hybridization on Co^+. This hybridization both reduces Pauli repulsion and fosters sigma donation into the 4*s* orbital on Co^+. Clusters $n = 3$ and $n = 4$ add at 90° to the $n = 1$ and 2 line of centers forming a planar system. The *s/d* hybridization is unfavorable for these clusters resulting in longer Co^+–C bond lengths and substantially reduced binding energies. To $n = 5$ and 6 ligands probably complete a pseudo octahedral complex and are very weakly bound, perhaps defining a second solvation shell. An impurity contributed substantially to the experimental peak at $m/z = 123$ corresponding to $Co^+(CH_4)_4$. The impurity was tentatively identified as $O_2Co^+(CH_4)_2$ and experimental protocals were developed to eliminate its impact on the data reported here. It is suggested this impurity could be responsible for published guided ion beam results that found a substantially larger binding energy for $n = 4$ than for $n = 3$ in contrast to what is reported here. (Int J Mass Spectrom 204 (2001) 281–294) © 2001 Elsevier Science B.V.

Keywords: Sigma bond activation; Transition metal; Cobalt; Methane; Density function theory

1. Introduction

The search for a method of controlled activation of the C–H bond in methane has been on going for many years due to its immense technological importance [1,2]. It is also of substantial fundamental importance as an alkane C–H bond prototype that is susceptible to high level electronic structure calculations. Transition metals are traditionally chosen as activation agents [1–3] although bare atomic transition metal atoms are known to be unreactive [3] due to their filled, repulsive 4*s* orbital (for first row metals). However, singly charged transition metal atoms have been successfully used to activate C–H bonds in C_3 and larger alkanes and many important experimental and theoretical studies have been reported [4]. Although the kinetics [5] and dynamics [6] of certain reactions have been explored, the dominant tool used to probe sigma bond activation has been thermochemistry; the guided beam method developed by Armentrout and coworkers [7] and the equilibrium method used by our group [8].

* Corresponding author. E-mail: bowers@chem.ucsb.edu.

[1] Current address: Department of Chemistry, Pohang University of Science and Technology, South Korea.

PII S1387-3806(00)00357-2

Activating the C–H bond in methane is a daunting task since the generic reaction

$$M^+ + CH_4 \rightarrow M^+CH_2 + H_2 \quad (1)$$

is at least 18 kcal/mol endothermic for the first row transition metals [9], although simple insertion into the C–H bond is closer to thermoneutral [9]. It was surprising, then, when the following reaction was observed [10]:

$$Ti^+ + 3CH_4 \rightarrow Ti^+(C_3H_{10}) + H_2 \quad (2)$$

and temperature dependence studies indicated it was near thermoneutral. Although the complete details of the mechanism remain to be proven [11], it is fairly certain that sequential clustering of three CH_4 ligands preceeds the loss of H_2. This kind of "cluster assisted" or "ligand assisted" activation mechanism was first observed [12] for insertion of Sc^+ into H_2. Subsequently, we found the $CpCo^+$ ion also activates CH_4 in a formal cluster assisted way

$$CpCo^+ + 2CH_4 \rightarrow Co^+(C_7H_{11}) + H_2 \quad (3)$$

although the mechanism is complex and involves the Cp ring [13].

Our studies of activation of the H–H bond in hydrogen by first row metal ions strongly indicate that complete activation is not required for substantial information to be obtained on the factors that govern the activation process [14,15]. In a similar way, we expect much information to be gained from systematically studying sequential clustering of CH_4 ligands even if complete activation is not observed. In this article we are revisiting a system that has been investigated previously: the sequential clustering of CH_4 ligands to Co^+. The bond dissociation energies for addition of the first two CH_4 ligands have been measured by equilibrium methods [16] and addition of the first four CH_4 ligands by the guided ion beam method [17]. High level theory has also been applied [17,18]. There is good agreement between the equilibrium and guided ion beam results and theory for the first two clusters. For cluster three and especially four something interesting appears to be happening. According to the guided ion beam experiment, the $Co^+(CH_4)_n$ bond energy drops from ~25 kcal/mol for $n = 2$ to ~9.4 kcal/mol for $n = 3$ and then rises again to ~15.4 kcal/mol for $n = 4$. This is very unusual behavior. Usually a monotonic (sometimes pairwise) decrease in binding energy occurs as common weak field ligands are added (H_2 or CH_4) due to either steric effects or to the fact that the prime bonding sites (orbitals) have been taken by prebound ligands. In the case of $V^+(H_2)_n$, a significant increase for $n = 6$ over $n = 5$ was observed and shown to be due to a spin change on the central V^+ metal [19,20]. In the $Co^+(CH_4)_n$ system, the increase was also observed in the theoretical calculation [17] and ascribed to a hybridization effect not a spin change. Since hybridization effects usually account for only 1 or 2 kcal/mol, this was a significant finding. Because we were embarking on a systematic study of CH_4 ligation to first row metal ions we felt it important to confirm this result. Our findings are given here, along with a new set of detailed electronic structure calculations. Both experiment and theory are at variance with the earlier results. Reasons are suggested for the differences observed in the two sets of experiments.

2. Methods

2.1. Experimental methods

Experimental details on the method and instrument have been given previously [12,21,22]. The Co^+ ions were formed either in a glow discharge source using Ar as a buffer gas or by electron impact on $Co(CO)_3NO$. Indentical results were obtained from both sources. The Co^+ ions were mass selected by a quadrupole mass filter and injected into a drift cell containing the CH_4 reaction gas (typical pressures 1–5 Torr). The ions drift under a weak electric field that does not measurably perturb their thermal energies and rapidly come to equilibrium:

$$Co^+(CH_4)_{n-1} + CH_4 \rightleftharpoons Co^+(CH_4)_n \quad (4)$$

The cell temperature is variable from 80 to 850 K and equilibrium constants were measured over this range

$$K_p^0 = \frac{Co^+(CH_4)_n(760)}{Co^+(CH_4)_{n-1}P_{CH_4}} \quad (5)$$

where P_{CH_4} is the pressure of CH_4 in Torr, (760) Torr normalizes to standard state conditions and $Co^+(CH_4)_n$, $Co^+(CH_4)_{n-1}$ are the measured intensities of the ions. The standard state free energy is then calculated

$$\Delta G_T^0 = -RT \ln K_p^0 \quad (6)$$

and enthalpies and entropies determined by plotting ΔG_T^0 versus T:

$$\Delta G_T^0 = \Delta H_T^0 - T\Delta S_T^0 \quad (7)$$

where ΔH_T^0 and ΔS_T^0 are the intercept and slope of the plot, respectively. These quantities are valid over the temperature range of the experiment. To get true bond dissociation energies (ΔH_0^0), extrapolations using statistical mechanics methods and theoretically determined structures and vibrational frequencies are accomplished.

The injection energy was normally kept low (<10 eV), resulting in a typical mass spectrum shown in Fig. 1(a). However, when the Co^+ injection energy was raised to 30 eV a new series of peaks arose corresponding to the equilibria

$$CH_3Co^+(CH_4)_{n-1} + CH_4 \rightleftharpoons CH_3Co^+(CH_4)_n \quad (8)$$

[Fig. 1(b)]. The ratio of ions arising from CH_3Co^+ to those from Co^+ is given as a function of injection energy in Fig. 2. The mechanism of formation CH_3Co^+ is complex and will be discussed elsewhere [23]. In this article only the equilibrium shown in Eq. (8) will be dealt with.

A number of checks were done to ensure equilibrium was established for all systems. For example, Eq. (5) requires that the ratio $Co^+(CH_4)_{n-1}/Co^+(CH_4)_n$ be independent of reaction time for a fixed pressure P_{CH_4}. This condition was met for almost all of the equilibria reported here. However, a dramatic departure from time independence of this ratio was observed for $n = 4$. An example is given for several pressures at $T = 250$ K in Fig. 3(a). In this case, the relative intensities of $m/z = 123$ [nominally $Co^+(CH_4)_4$] increase with time relative to the intensity of $m/z = 107$ [nominally $Co^+(CH_4)_3$] indicating an irreversible process is either depleting $m/z = 107$, forming $m/z = 123$ or both. In order to assertain if an irreversible formation of $m/z = 123$ was the problem, we did a similar plot of the ratio of $m/z = 123$ to $m/z = 91$ [nominally $Co^+(CH_4)_2$], shown in Fig. 3(b). Since this ratio still shows a problem exists and since $Co^+(CH_4)_2$ passed all of the equilibrium tests for time and pressure dependence, the problem must be with $m/z = 123$. Hence, a

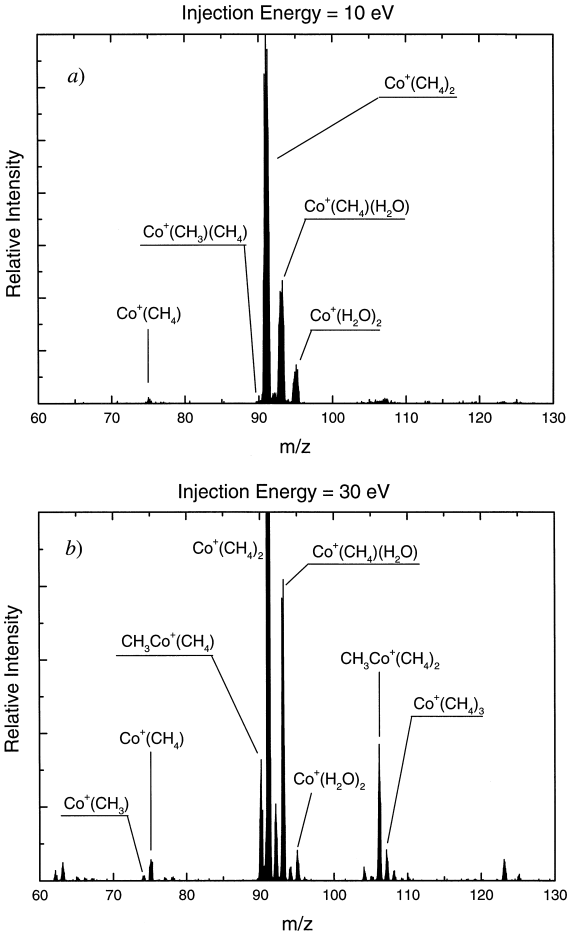

Fig. 1. (a) Typical mass spectrum of cobalt-methane cluster ions. The bare cobalt ion was injected with 10 eV kinetic energy into the reaction cell. The temperature of the reaction cell is 300 K, and the pressure of methane is 2 Torr. (b) Spectrum is obtained by injecting Co^+ with 30 eV kinetic energy. The temperature of the reaction cell is 300 K, and the pressure of methane is 2 Torr.

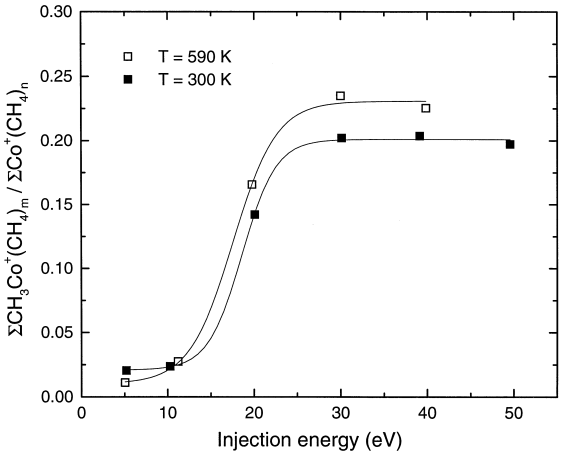

Fig. 2. Plot of the ratio of $\Sigma CH_3Co^+(CH_4)_m/\Sigma Co^+(CH_4)_n$ as a function of injection energy of Co^+, where $m = 1$–2 and $n = 0$–3.

protocol had to be established to determine the equilibrium constant for formation of $Co^+(CH_4)_4$ in the presence of this unknown reaction.

Of importance is the fact that the interfering reaction is relatively slow, whereas establishing equilibrium for simple ligand addition is immeasurably fast under our experimental conditions. Hence, if the apparent equilibrium constant (or ratio of peak intensities) is measured as a function of time and extrapolated to $t = 0$, this asymptotic value should give the true equilibrium constant. Examples are given in Fig. 4. As a further safeguard, the ΔG_T^0 values obtained in this way were then remeasured at a series of pressures which were also extrapolated to $P_{CH_4} = 0$. This safeguard allows elimination of other possible problems [like collision-induced dissociation (CID) following the exit hole of the cell]. These doubly extrapolated values of ΔG_T^0 are then plotted versus temperature, and yield a linear plot as shown in Fig. 5.

We have attempted to unambiguously identify the impurity source at $m/z = 123$. An obvious choice is oxygen [either $OCo^+(CH_4)_3$ or $O_2Co^+(CH_4)_2$] since both the O atom and CH_4 have the same nominal mass. One possible source of oxygen is water but the reaction

$$Co^+ + H_2O \rightarrow Co\,O^+ + H_2 \qquad (9)$$

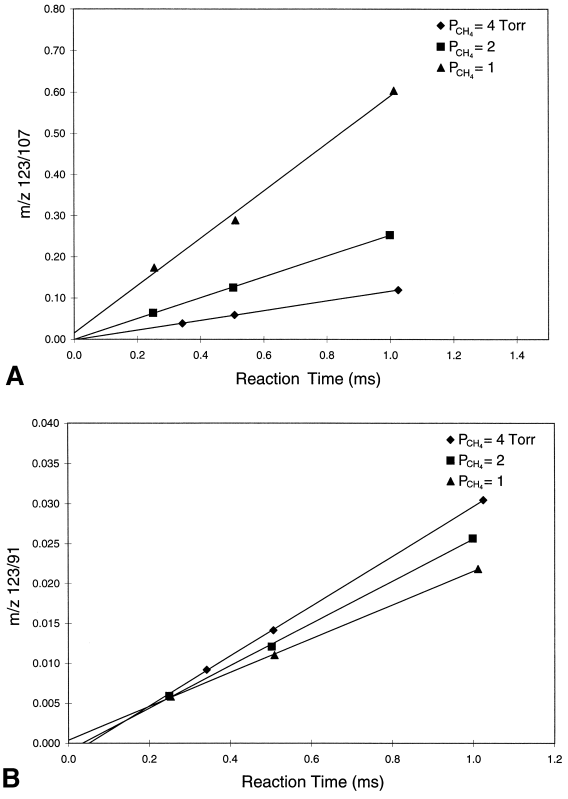

Fig. 3. (a) Plot of the ratio of peaks 123/107 vs. reaction time at 250 K at several different methane pressures. (b) Plot of the ratio of peaks 123/91 vs. reaction time at 250 K at several different methane pressures.

is strongly endoergic and presumably remains so when Co^+ is ligated with CH_4. Further, as the data in Fig. 1 show, water readily clusters with Co^+ in the presence of CH_4 and gives no indication a reaction like Eq. (9) is occurring.

Another possibility is direct clustering of O_2 to Co^+. In this instance, the most likely scenarios are

$$Co^+(CH_4)_2 + O_2 \rightarrow O_2Co^+(CH_4)_2 \qquad (10)$$

$$Co^+(CH_4)_3 + O_2 \rightarrow O_2Co^+(CH_4)_2 + CH_4 \qquad (11)$$

Under the conditions of the experiment, reaction (10) can be ruled out since $Co^+(CH_4)_3$ is much more abundant than $Co^+(CH_4)_2$ suggesting that reaction (11) is responsible. One of the interesting clues in the mystery is the fact the impurity contamination of $m/z = 123$ is reduced as temperature is reduced and

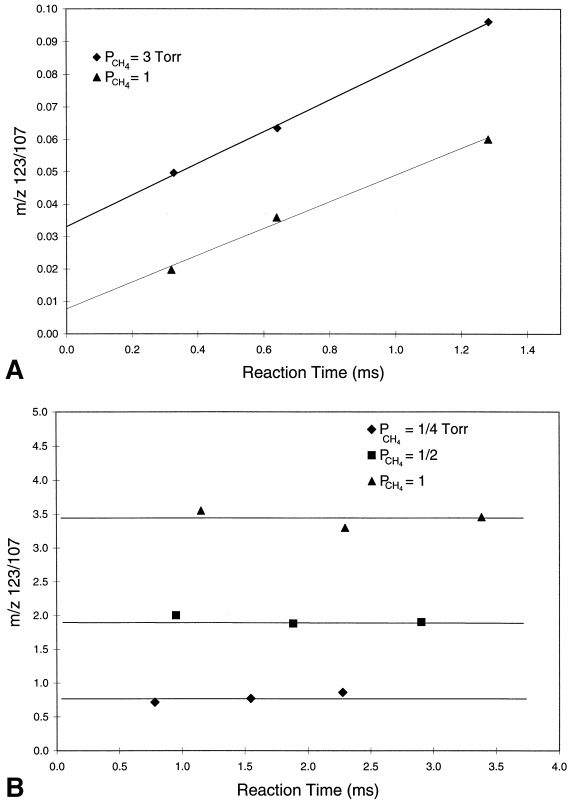

Fig. 4. (a) Plot of the ratio of peaks 123/107 vs. reaction time at 200 K. The asymptotic values at $t = 0$ give the true equilibrium ratios (see text). (b) Plot of the ratio of peaks 123/107 vs. reaction time at 125 K. In addition to the CH_4 there was 2 Torr helium bath gas. The equilibrium ratio is almost time invariant and near proportional to the methane pressure.

finally disappears below $T = 125$ K (see Figs. 3 and 4). This result is qualitatively consistent with a ligand switching reaction favoring the impurity contribution and a clustering reaction forming the true $Co^+(CH_4)_4$ product

$$Co^+(CH_4)_3 + CH_4 \rightleftharpoons Co^+(CH_4)_4 \qquad (12)$$

For ligand switching, $\Delta S_T^0 \cong 0$ and could be positive while for the clustering reaction $\Delta S_T^0 \cong -25$ cal mol^{-1} K^{-1}. Hence, for every 100 K decrease in temperature, the ΔG_T^0 for reaction (12) decreases by about 2.5 kcal/mol relative to that for reaction (11), apparently, eventually dominating below 125 K.

The evidence and related arguments given here are circumstantial and do not prove reaction (11) is

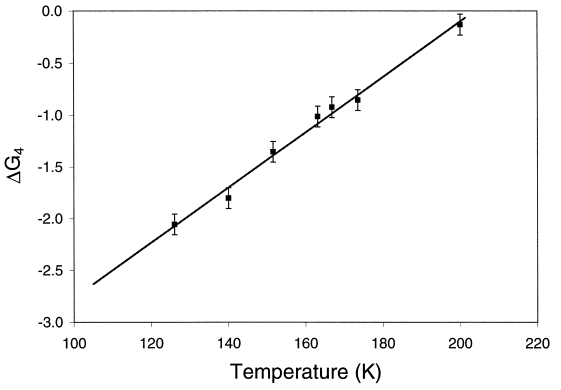

Fig. 5. Plot of ΔG_T^0 vs. temperature for the association reaction $Co^+(CH_4)_3 + CH_4 \rightleftharpoons Co^+(CH_4)_4$. We first extrapolate ΔG_T^0 to zero reaction time, $\Delta G_{T,t=0}^0$, then extrapolate $\Delta G_{T,t=0}^0$ to zero pressure, $\Delta G_{T,t=0,P=0}^0$. The error bar is the maximum uncertainty with above extrapolations.

responsible. To do so is an almost impossible task due to the mass degeneracy of O atom and CH_4. We did notice a very slight irreversible reaction occurring in the *m/z* 107/91 ratio above 250 K which indicates that a small amount of ligand switching could be occurring with $Co^+(CH_4)_2$:

$$Co^+(CH_4)_2 + O_2 \rightarrow O_2Co^+(CH_4) + CH_4 \qquad (13)$$

However, as we will show, reaction (13) is energetically less favorable than reaction (11) by about 18 kcal/mol and reaction (13) appears to have no effect on the results obtained. We did extrapolate the ΔG_T^0 values to both $T = 0$ and $P = 0$ for this system just to be sure, however.

2.2. Theoretical

All calculation were carried out at the density functional theory (DFT) level using the unrestricted open shell B3LYP functional [24,25] and the GAUSSIAN98 program package [26]. For carbon and hydrogen, the 6-31G(*d*,*p*) basis was used. In order to ensure basis set superposition error were minimized, we first used the DZVP basis set [27] for cobalt, which is a [5*s*3*p*2*d*] contraction of (15*s*9*p*5*d*) primitive set. This basis led to unacceptable imaginary frequency problems for the weak Co^+–CH_4 clustering modes.

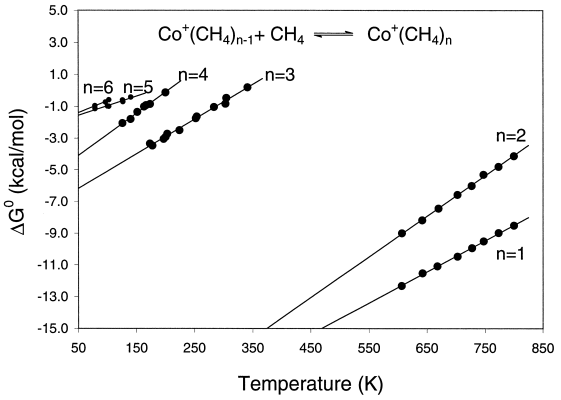

Fig. 6. Plot of experimental ΔG^0 vs. temperature for the association reactions $Co^+(CH_4)_{n-1} + CH_4 \rightleftharpoons Co^+(CH_4)_n$.

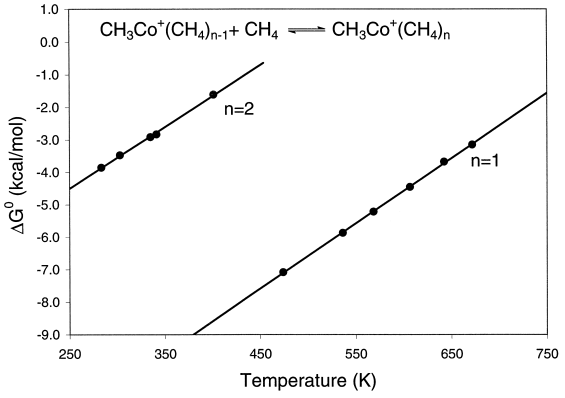

Fig. 7. Plot of experimental ΔG^0 vs. temperature for the association reaction $CH_3Co^+(CH_4)_{n-1} + CH_4 \rightleftharpoons CH_3Co^+(CH_4)_n$.

Consequently, we also used the (14*s*11*p*6*d*3*f*)[8*s*6*p*4*d*1*f*] Wachters basis set [28] which essentially eliminated this problem. Full geometry optimization and frequency analyses are performed on all $Co^+(CH_4)_n$ clusters using this higher order basis set. The DZVP basis was used for the $CH_3Co^+(CH_4)_n$ system.

3. Results

3.1. Experimental

The methods discussed previously were used to obtain accurate values of ΔG_T^0 over a wide temperature range for sequential clustering of up to six CH_4 ligands about the Co^+ core ion and two CH_4 ligands about the $CoCH_3^+$ core ion. These data are plotted in Figs. 6 and 7 and the ΔH_T^0 and ΔS_T^0 results extracted from Figs. 6 and 7 are summarized in Tables 1 and 2. The $n = 4$ data in Fig. 6 are restricted to $T \leq 200$ for reasons given previously.

One striking feature of the data in Fig. 6 is the pairwise similarity in both ΔH_T^0 (intercepts at $T = 0$) and $-\Delta S_T^0$ (slopes); $n = 1$ and 2 are strongly bound, $n = 3$ and 4 have intermediate bonding energies and $n = 5$ and 6 are very weakly bound. In addition, the values of ΔS_T^0 are substantially greater (i.e. less negative with shallower slopes) for $n = 5$ and 6. There is no evidence that the $n = 4$ bonding energy is greater than the $n = 3$. In fact, the opposite is true (Table 1).

The covalently bound CH_3 radical acts qualitatively like a CH_4 ligand. The first CH_4 ligand is bound relatively strongly to $CoCH_3^+$ and the second one significantly less strongly. There are, however definite quantitative differences between $CoCH_3^+$ and

Table 1
Experimental results for the reactions $Co^+(CH_4)_{n-1} + CH_4 \rightleftharpoons Co^+(CH_4)_n$

n	$-\Delta H_T^{0a}$ (kcal/mol)	$-\Delta S_T^{0b}$ (cal mol^{-1} K^{-1})	Temperature range (K)
1	24.2	19.7	700 ± 100
2	24.6	25.7	700 ± 100
3	7.3	21.9	250 ± 100
4	5.4	26.7	150 ± 50
5	~2	~12	115 ± 35
6	~2	~13	90 ± 10

[a] Estimated uncertainty of 1%–2% except for $n = 5$, 6.
[b] Estimated uncertainty of 1%–2%.

Table 2
Experimental results for the reactions $CH_3Co^+(CH_4)_{n-1} + CH_4 \rightleftharpoons CH_3Co^+(CH_4)_n$ for $n = 1$, 2

n	$-\Delta H_T^{0a}$ (kcal/mol)	$-\Delta S_T^{0b}$ (cal mol^{-1} K^{-1})	Temperature range (K)
1	16.6	20.1	550 ± 100
2	9.3	19.0	340 ± 60

[a] Estimated uncertainty between 1% and 2%.
[b] Estimated uncertainty between 1% and 2%.

Co^+CH_4. That fact will be briefly commented on later in the article.

3.2. Theoretical

A thorough study has been made to locate the lowest energy states of the $Co^+(CH_4)_n$ systems. Although these systems have been discussed previously [17,18], we take a somewhat different approach and so a brief accounting of our findings are useful. We will do so system by system.

3.2.1. Co^+CH_4

Both η^2 and η^3 configurations were explored. The lowest energy state was determined to be $^3B_2$ of C_{2v} symmetry but the $^3A_2$ state of C_{3v} symmetry was only 0.7 kcal/mol higher in energy (see Fig. 8). The bond energies are given in Table 3. The lowest energy $^3B_2$ η^2 state has a bond energy of 22.9 kcal/mol in excellent agreement with experiment. Choosing the x axis as the bonding axis, the Co^+ electron configuration is

$$a_1(d_{x^2-y^2})^2 b_1(d_{xz})^2 a_2(d_{yz})^2 b_2(d_{xy})^1 a_1(d_{z^2})^1$$

which retains the low energy ^3F state for the metal center. The primary interactions, as determined from natural bond orbital [29,30] population analyses (Table 4), are donation from the a_1 symmetry orbital on CH_4 into the vacant 4s orbital on Co^+ and a small donation from the b_2 symmetry orbital on CH_4 into the singly occupied d_{xy} orbital on Co^+. These charge transfer interactions result in a small elongation of the C–H bond (0.033 Å) and reduction in the vibrational frequencies of the proximate C–H bonds by between 100 and 200 cm^{-1}. The 4s orbital also (partially) hybridizes with the doubly occupied $d_{x^2-y^2}$ orbital [31] generating two positive bonding effects: reduction of Pauli repulsion by shifting electron density to the y axis and improving overlap with the a_1 orbital on CH_4 by elongating the 4s orbital along the x axis.

An $^3A_2$ state of C_{2v} symmetry is found to be 3 kcal/mol higher in energy than the $^3B_2$ state. This state orients the singly occupied d_{z^2} orbital toward the η^2 bound methane. Although a number of factors

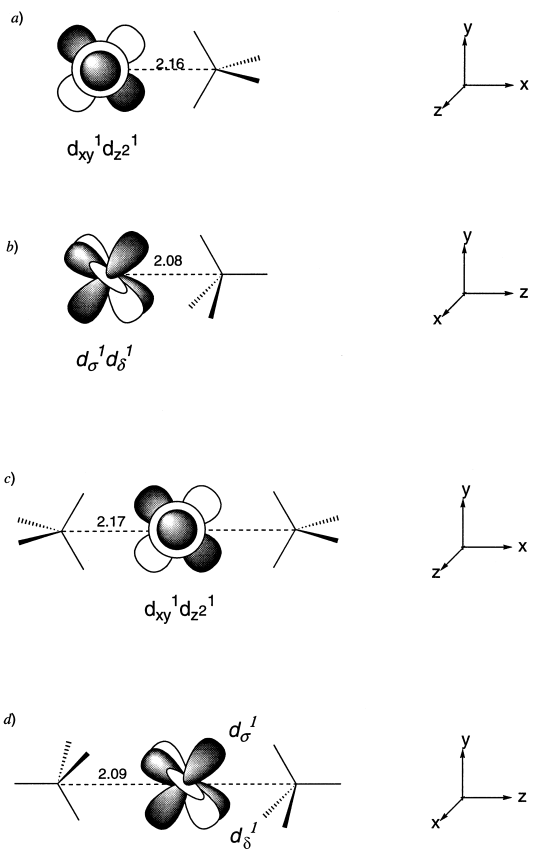

Fig. 8. Geometry of the $Co^+(CH_4)_n$ clusters: (a) $n = 1$ with C_{2v} symmetry, where x is the principal axis; (b) $n = 1$ with C_{3v} symmetry, where z is the principal axis; (c) $n = 2$ with D_{2h} symmetry; and (d) $n = 2$ with C_{3v} symmetry. The orientations of the singly occupied orbitals on Co^+ are shown schematically.

Table 3
Comparison of bond dissociation energies ($-\Delta H_0^0$) between experiment and theory for the reactions $Co^+(CH_4)_{n-1} + CH_4 \rightleftharpoons Co^+(CH_4)_n$ and $CH_3Co^+(CH_4)_{m-1} + CH_4 \rightleftharpoons CH_3Co^+(CH_4)_m$

	$-\Delta H_0^0$ (kcal/mol)	
	Experiment	Theory
$n = 1$	23.1 (21.4)[a]	22.9 (21.4)[ab]
$n = 2$	25.3 (23.0)[a]	22.1 (23.0)[ab]
$n = 3$	7.3 (9.4)[a]	5.4 (~9.2)[ab]
$n = 4$	5.2 (15.4)[a]	2.2 (~16.1)[ab]
$m = 1$	17.2	13.7
$m = 2$	9.2	7.1

[a] From [17].
[b] D_e not D_0.

Table 4
Natural bond orbital population of Co^+ in $Co^+(CH_4)_n$ clusters

Cluster	State	4s	$4p_x$	$4p_y$	$4p_z$	d_{xy}	d_{xz}	d_{yz}	$d_{x^2-y^2}$	d_{z^2}
Co^+CH_4	η^2C_{2v} $^3B_2$	0.1028	0.0040	0.0026	0.0013	1.0221	1.9927	2.0000	1.9281	1.0064
	η^2C_{2v} $^3A_2$	0.0499	0.0012	0.0023	0.0045	1.0000	1.9951	1.9898	1.9948	1.0031
	η^3C_{3v} $^3A_2$[a]	0.1033	0.0041	0.0041	0.0013	1.6750	1.3360	1.3360	1.6750	1.9105
	η^3C_{3v} $^3A_2$[b]	0.0955	0.0040	0.0040	0.0015	1.6798	1.3247	1.3247	1.6798	1.9203
$Co^+(CH_4)_2$	η^2D_{2h} $^3B_{1g}$	0.2419	0.0081	0.0040	0.0017	1.0487	1.9875	1.9999	1.8736	1.0104
	η^3D_{3d} $^3A_{2g}$[a]	0.2414	0.0060	0.0060	0.0017	1.6988	1.3272	1.3272	1.6988	1.8432
	η^3D_{3d} $^3A_{2g}$[b]	0.2328	0.0058	0.0058	0.0018	1.7075	1.3040	1.3040	1.7075	1.8500
$Co^+(CH_4)_3$	η^2D_3 $^3A_2$	0.1719	0.0079	0.0079	0.0034	1.5788	1.4502	1.4502	1.5788	1.9477
	η^2C_{2v} $^3A_2$	0.2037	0.0042	0.0088	0.0061	1.0430	1.9948	1.9869	1.8984	1.0476
$Co^+(CH_4)_4$	η^2D_{2h} $^3B_{1g}$[c]	0.1880	0.0040	0.0095	0.0081	1.0418	1.9928	1.9887	1.9039	1.0823
	η^2C_s $^3A''$	0.1321	0.0091	0.0076	0.0073	1.2289	1.3503	1.6866	1.9659	1.8005
	η^2D_{2h} $^3B_{1g}$[d]	0.1249	0.0088	0.0088	0.0033	1.0550	1.9874	1.9874	1.9915	0.9930

[a] With two singly occupied d_σ and d_δ orbitals toward the η^3 hydrogens, also see Fig. 8(b) and (d).
[b] With two doubly occupied d_σ and d_δ orbitals toward the η^3 hydrogens.
[c] Wtih two sets Co^+–C bonds, see Fig. 9(c).
[d] With four equivalent Co^+–C conds (2.52 Å).

cause it to be higher in energy, the primary one is a lack of hybridization with the 4*s* orbital.

The lowest energy η^3 state is $^3A_2$ in C_{3v}. Actually there are two states separated by 1.7 kcal/mol. In both states, the d_{z^2} orbital is doubly occupied and is parallel to the C_3 bonding axis. In this case the d_{z^2} orbital does hybridize with the 4*s* orbital again leading to the dual benefits of reduced Pauli repulsion and increased overlap with the a_1 symmetry orbital on CH_4. The difference in energy of the two $^3A_2$ states results from the orientation of the two singly occupied d_σ and d_δ orbitals on Co^+: (1) toward the η^3 hydrogens (lower energy) or (2) away from the η^3 hydrogens (higher energy).

3.2.2. $Co^+(CH_4)_2$

The ground state is found to be a $^3B_{1g}$ state of D_{2h} symmetry as previously found by Haynes et al. [17] (Fig. 8). The bonding of the second methane is identical to the first on the opposite side of the Co^+ center. A bond dissociation energy of 22.1 kcal/mol is calculated in good agreement with experiment. It is worth noticing that the experimental bond dissociation energy (BDE) is 2.2 kcal/mol larger for the second CH_4 ligand than for the first whereas theory predicts a slightly lower BDE for the second versus the first. This is probably a result of an overestimation of the first BDE by the DFT method, something that we have previously observed [32]. The dual Hartree-Fock/modified coupled pair functional procedure used by Haynes et al. [7] did find a slightly larger second BDE relative to the first.

We also explored η^3 complexes with the lowest energy form being a $^3A_{2g}$ state of D_{3d} symmetry (Fig. 8). The bonding of the second CH_4 ligand was the same as the first in both cases. Again, a bonding energy only slightly smaller than the $^3B_{1g}$ state was found.

3.2.3. $Co^+(CH_4)_3$

We found two configurations with essentially the same energy for this cluster (Fig. 9). The first is a near T-shape with the third CH_4 ligand approaching at 90° to the line of centers of the η^2 C_{2v} $Co^+(CH_4)_2$ structure. In this case the Co^+ ion retains its same electron configuration and *s/d* hybridization. This results in a C_{2v} structure with one long Co^+–C bond (2.57 Å) and two short bonds (2.23 Å).

The second structure is trigonal with D_3 symmetry. Actually, there are two chiral isomers with the CH_4 ligands rotated ±31° around the Co^+–C bonds from a "planar" D_{3h} structure. In this instance, the electron configuration is

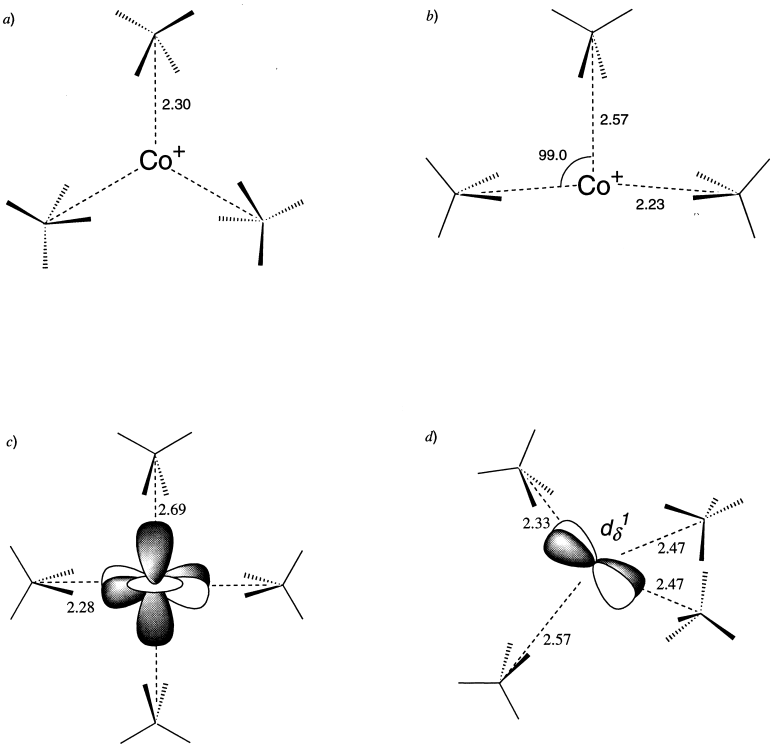

Fig. 9. Geometry of the $Co^+(CH_4)_n$ clusters: (a) $n = 3$ with D_3 symmetry; (b) $n = 3$ with C_{2v} symmetry; (c) $n = 4$ with D_{2h} symmetry; and (d) $n = 4$ with C_s symmetry.

$$a_1(d_{z^2})^2 e_1(d_{x^2-y^2} \pm d_{xz})^2 e_1(d_{xy} \pm d_{yz})^2 e_2(d_{x^2-y^2} \pm d_{xz})^1 e_2(d_{xy} \pm d_{yz})^1$$

where the upper sign corresponds to positive rotation and the lower sign to negative rotation about the Co^+–C bonds. The *z* axis is the principal rotation axis perpendicular to the plane containing the three CH_4 ligands. The two singly occupied orbitals are oriented to accept electron density from a pair of hydrogens on one of the CH_4 ligands while the doubly occupied orbitals are at right angles to minimize repulsion. Some *s/d* hybridization occurs with the d_{z^2} orbital to minimize repulsion but is less than either the C_{2v} structure or the $n = 1$ and 2 systems (Table 4). Similar structures are found by Haynes et al. [17] but with slightly different geometry and energies.

3.2.4. $Co^+(CH_4)_4$

We found the ground state to be $^3B_{1g}$ with D_{2h} symmetry (Fig. 9). The cluster is essentially the $n = 2$ ground state with the third and fourth CH_4 ligands approaching at 90° in the molecular plane. The electron configuration is unchanged from the $n = 2$ cluster. Two short (2.28 Å) and two long bond (2.69 Å) bonds are formed. The binding energy of 2.2 kcal/mol is somewhat smaller than experiment (5.2 kcal/mol), but that is not unexpected for a molecule of this size at this level of theory.

A second stable structure was located with C_s symmetry at quasitetrahedral geometry. It has one short bond (2.33 Å), two intermediate (2.47 Å) and one long bond (2.57 Å). The singly occupied orbitals are oriented to minimize repulsion. The long bond CH_4 ligand has a doubly occupied d_σ orbital pointed directly toward it.

A cluster with initial D_{4h} symmetry was also considered, that slightly distorts to D_{2h} due to the Jahn-Teller effect. For the electron configuration

$$b_{2g}(d_{xz})^2 b_{3g}(d_{yz})^2 a_g(d_{x^2-y^2})^2 b_{1g}(d_{xy})^1 a_g(d_{z^2})^1$$

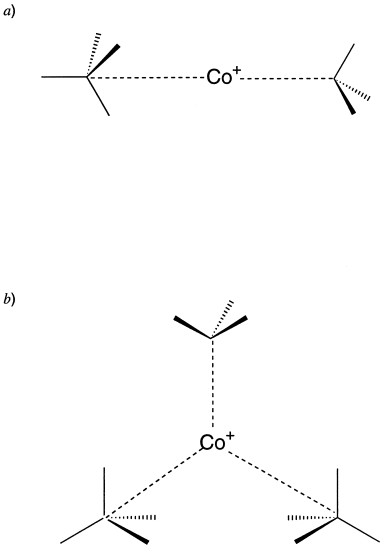

Fig. 10. Geometry of the $CH_3Co^+(CH_4)_n$ clusters: (a) $n = 1$ with C_{3v} symmetry and (b) $n = 2$ with C_s symmetry.

the z axis is perpendicular to the molecular plane and four equivalent bond lengths of 2.52 Å were found. This cluster is unbound relative to loss of CH_4 by 0.4 kcal/mol. When the electron configuration is changed to that reported by Haynes et al. [17]

$$a_g(d_{z^2})^2 b_{2g}(d_{xz})^2 a_g(d_{x^2-y^2})^2 b_{1g}(d_{xy})^1 b_{3g}(d_{yz})^1$$

the bond length reduces to 2.44 Å but the cluster is even more unstable at 1.5 kcal/mol.

3.2.5. $CH_3Co^+(CH_4)$

The lowest energy structure was found to be a $^4A_2$ state with C_{3v} symmetry (Fig. 10), a $3d^7 4s^1$ electron configuration, with a Co^+–CH_3 bond length of 1.93 Å and a Co^+CH_4 bond length of 2.38 Å. A calculated value for the Co^+–CH_4 bond dissociation energy of 13.7 kcal/mol is in acceptable agreement with experiment, 17.2 kcal/mol. Two η^2-bound CH_4 states were found to be stable as well (C_s symmetry) but they were 2.9 and 5.3 kcal/mol higher in energy. The lowest lying doublet state was significantly higher in energy.

3.2.6. $CH_3Co^+(CH_4)_2$

The lowest energy structure has both CH_4 ligands η^3 bound in a $^3A''$ state of C_s symmetry (Fig. 10). The pseudo C_{2v} structure has a Co^+–CH_3 bond length of 1.93 Å identical to the $CH_3Co^+(CH_4)$ cluster. The two Co^+–CH_4 bond lengths are 2.51 Å indicate (near) identical bonding. The calculated bond dissociation energy of 7.1 kcal/mol is in acceptable agreement with experiment (9.2 kcal/mol).

4. Discussion

Good agreement is found between the theoretical and experimental bond energies for $n = 1$–4. In particular, the first two are theoretically predicted to be relatively strong as observed and the third about 17 kcal/mol weaker, again as observed. Finally, the fourth is predicted to be weaker still by several kcal/mol, again confirmed by experiment. The bonding in the entire sequence of structures appears to be determined by the bonding of the first CH_4 ligand. The lowest energy structure is η^2 with significant $4s/3d_{x^2-y^2}$ hybridization. The hybridization both reduces repulsion along the bonding x axis and promotes increased electron donation from the two proximate C–H σ bonds into the (nearly) vacant 4s orbital. The second CH_4 ligand binds identically on the opposite site of the metal ion and enjoys the same benefits of the *s/d* hybridization. The third CH_4 must approach at right angles to the first two. The most probable structure of this species is T-shaped [Fig. 9(b)] although the barrier to rearrangement to form the trigonal structure [Fig. 9(a)] may not be large. In the T-shaped structure the bonding of the first two CH_4 ligands is essentially identical to the dimer. The binding energy of the third ligand is negatively impacted by the existing *s/d* hybridization, and probably by steric hindrance. The net affect is a strong drop in binding energy from 25.3 to 7.3 kcal/mol and an elongated Co–C bond length (2.57 versus 2.23 Å). When the fourth CH_4 approaches it does so opposite the third with the same negative influences at play. The result is a slightly weaker bond (5.2 kcal/mol) and slightly longer bond (2.69 Å). These effects are almost surely due to the increased steric effects as the strongly bound ligands $n = 1$ and $n = 2$ can no

longer bend away from $n = 3$ and are forced back into a linear alignment with the Co^+ metal center.

There are, as mentioned in the previous section, other possible structures for each of the clusters and at this level of theory the above scenario cannot be unambiguously posited. However, it does nicely rationalize all of the experimental observations and smoothly builds from the $n = 1$ cluster to $n = 4$ without either changing the electron configuration on Co^+ or requiring any structural rearrangement of the ligands as new ones are attached. These are compelling reasons to support this simple picture.

The addition of the next two CH_4 ligands, $n = 5$ and $n = 6$, probably occurs along the y axis perpendicular to the xz plane of the $n = 4$ cluster. A pseudo octahedral complex is probably formed but ligands 5 and 6 are very weakly bound and probably have a significantly longer Co^+–C bond length than $n = 3$ and 4. The increase in ΔS_T^0 by 10–15 entropy units (from −26 to −12) indicates the final two ligands have great freedom of motion consistent with their very small bonding energy. These are, in effect, in the second solvation shell.

The disagreement with the guided ion beam results for $n = 4$ is substantial. As pointed out in our experimental methods section, we discovered a persistent impurity contribution to the $m/z = 123$ peak, which is nominally $Co^+(CH_4)_4$. Although we cannot absolutely prove it, we feel the impurity is most likely $O_2Co^+(CH_4)_2$. In our experimental set up we did everything we could to eliminate O_2, including putting an oxygen getter in the cell inlet lines, yet the impurity persisted. Hence, even very small amounts of O_2 must be able to significantly affect the $m/z = 123$ peak. If this impurity is present in our system it might also be present in the guided ion beam instrument [17]. If so, the threshold they measure could be due to

$$O_2Co^+(CH_4)_2 \xrightarrow{Xe} O_2Co^+(CH_4) + CH_4 \quad (14)$$

instead of

$$Co^+(CH_4)_4 \xrightarrow{Xe} Co^+(CH_4)_3 + CH_4 \quad (15)$$

Although the analogy of CH_3 mimicking O_2 is far from perfect, we established that

$$CH_3Co^+(CH_4)_2 \xrightarrow{Xe} CH_3Co^+(CH_4) + CH_4 \quad (16)$$

would have a threshold of 17.2 kcal/mol which is similar to the measured guided ion beam threshold for formation of m/z 107 from m/z 123. Hence, reaction (14) may in fact be occurring in their instrument.

There are several unusual features in the cross section versus energy plot reported by Haynes et al. [17] for collisional dissociation of the ion at $m/z = 123$, i.e. $Co^+(CH_4)_4$, $O_2Co^+(CH_4)_2$, or less likely $OCo^+(CH_4)_3$. First, the appearance curve of $m/z = 91$ has noticeable structure in it, with a "kink" appearing near 0.8 eV suggesting a second process may be leading to products. This kink was not noted or commented on by Haynes et al. However, if our suggestion is correct and $m/z = 123$ is dominantly $O_2Co^+(CH_4)_2$, then the two overall processes forming $m/z = 91$ are

$$O_2Co^+(CH_4)_2 \xrightarrow{Xe} O_2Co^+ + 2CH_4 \quad m/z = 91 \quad (17a)$$

$$O_2Co^+(CH_4)_2 \xrightarrow{Xe} Co^+(CH_4)_2 + O_2 \quad m/z = 91 \quad (17b)$$

Although the detailed thermochemistry for reaction (17a) and (17b) is not known, Eq. (17a) probably has a higher threshold energy than Eq. (17b) since the ligand switching reaction (11) appears to facilly form $O_2Co^+(CH_4)_2$ but the ligand switching reaction (13) does not form appreciable amounts of $O_2Co^+(CH_4)$. Hence, the binding energy of O_2 to partially ligated Co^+ is probably of the order 20 ± 5 kcal/mol. Since loss of one CH_4 from $O_2Co^+(CH_4)_2$ requires 15.4 kcal/mol, reaction (17a) requires in excess of 30 kcal/mol. Hence, the observed threshold is due to reaction (17b) and the kink due to reaction (17a). This interpretation is in qualitative agreement with the observed data of Haynes et al.

The second unusual feature in the data of Haynes et al. is the fact that the cross section for appearance of $m/z = 75$ [i.e. $Co^+(CH_4)$] becomes larger than the cross section for appearance of $m/z = 91$ at center of mass, energies above 2 eV. For "sequential" threshold

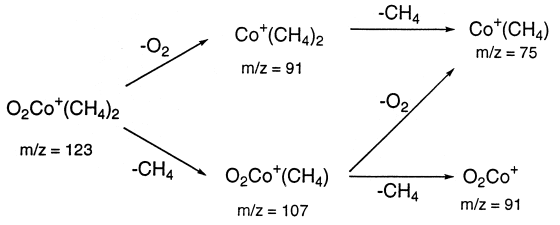

Scheme I

processes, this is a very unusual observation that suggests something special is occurring. Haynes et al. [17] suggest it could be due to the fact that $Co^+(CH_4)_3$ has two nearly energy degenerate structures [see Fig. 9(a) and (b)], that have different dissociation dynamics that could somehow explain this effect. If our interpretation is correct, $Co^+(CH_4)_3$ is not formed at all, and hence the structural isomer dissociation dynamics is a moot issue. If we have correctly identified the $m/z = 123$ ion as $O_2Co^+(CH_4)_2$, then the competitive dissociation reactions are given in Scheme 1.

When $m/z = 123$ dissociates, loss of CH_4 occurs forming $m/z = 107$ at lowest energies with a threshold according to Haynes et al. of 15.4 kcal/mol. According to our interpretation, the next threshold observed is loss of O_2 forming $m/z = 91$ at 21.8 kcal/mol. The threshold for forming $m/z = 75$ is a further 29 kcal/mol higher in energy and can come from either loss of O_2 from $O_2Co^+(CH_4)$ $m/z = 107$ or loss of CH_4 from $Co^+(CH_4)_2$, $m/z = 91$. This schematic mechanism could explain the fact that the abundance of $m/z = 75$ exceeds that of $m/z = 91$ at high energies if the Co^+–CH_4 bond strength is significantly larger than the Co^+–O_2 bond strength. If this is true now $m/z = 91$ will be preferentially depleted to form Co^+ at $m/z = 59$. We know the Co^+–CH_4 bond strength is 22.9 kcal/mol and it would not be unreasonable if the Co^+–O_2 binding energy were 5 kcal/mol less.

One troubling aspect remains. The modified coupled pair functional (MCPF) theoretical calculations of Haynes et al. indicate the fourth CH_4 ligand is much more strongly bound than the third. For reasons given above we think experiment conclusively indicates the fourth CH_4 is more weakly bound than the third. The DFT calculations reported here are in good agreement with experiment but not with the MCPF theoretical results. MCPF is a single reference configuration interaction (CI) method. For $n = 4$, Haynes et al. found the two singly occupied d orbitals on cobalt were d_{xy} and d_{yz}. This configuration does not correspond to the pure ^3F ground state of isolated Co^+. On the other hand, the DFT ground state had the singly occupied orbitals as d_{xy} and d_{z^2} which do correspond to the pure ^3F ground state of Co^+. In fact the lowest energy Co^+ configuration was unchanged for $n = 1$–4 in DFT. However, DFT is a single reference method with CI only indirectly handled in the parameterization. Consequently, we decided to do the following test.

First we generated complete active space self consistent field (CASSCF) wave functions with the $3d$ orbitals as the active space using the ground state found by Haynes et al. (four equal Co^+–CH_4 bonds) and the DFT ground state found here (two long and two short Co^+–CH_4 bonds). The state with four equivalent bonds generated a CI eigenvector

$$\Psi_1 \cong 0.94 d_{xy} d_{yz} - 0.33 d_{x^2-y^2} d_{xz} \quad (18)$$

where the noted d orbitals are singly occupied and the remaining doubly occupied. For the two long bond/two short bond state

$$\Psi_2 \cong 1.0 d_{xy} d_{z^2} \quad (19)$$

The orientation of the xyz axes are different in both cases but the same as previously noted (Fig. 8 and [17]). We then did single point single double (CISD) calculations and found the state corresponding to Ψ_1 3 kcal/mol higher in energy than the state corresponding to Ψ_2. A Wachters (f)/6-31G(d,p) basis was used in the calculations. These results are virtually identical to the DFT calculations previously discussed where the state with four equal Co^+–CH_4 bonds was 4.0 kcal/mol higher in energy than the one with two long and two short Co^+–CH_4 bonds.

The above mentioned results are in line with what would have been predicted qualitatively for the different orbital populations. In the DFT ground state,

the singly occupied d_{xy} orbital nicely overlaps with the two pairs of proximate C–H bonds [see the $n = 2$ structure in Fig. 8(c)] whereas the singly occupied d_{z^2} orbital is directed at the two methanes with the long Co^+–CH_4 bonds. The first interaction is stabilizing due to (a small) electron donation from the proximate CH_4 ligands into d_{xy} whereas the orientation of the d_{z^2} orbital minimizes metal–ligand repulsion.

For the state with four equivalent Co^+–CH_4 bonds, the d_{xy} and d_{yz} orbitals are singly occupied. The four CH_4 ligands are in the *xy* plane [17] and the lobes of the d_{xy} orbital are directed toward them in an η^2 configuration. This configuration is very mildly stabilizing but the longer Co^+–CH_4 bond lengths probably make it less so than the long/short configuration discussed above. (2.45 Å bond length for this case and 2.28 Å for the short bond in the prior case.)

The orientation of the d_{yz} orbital does minimize repulsion but apparently not as effectively as the d_{z^2} orbital in the long/short bonding case described previously due to the proximity of all four CH_4 ligands in the equal bond structure. In any case there is no indication that the $d_{xy}d_{yz}$ electron configuration should lead to a greater than 10 kcal/mol stabilization over the $d_{xy}d_{z^2}$ configuration as suggested by the calculations of Haynes et al.

In summary, the DFT calculations reported here are in good quantitative agreement for $n = 1$–4 with the experimental binding energies. Similar agreement for $n = 1$ and 2 is obtained with the MCPF calculations of Haynes et al. but for $n = 3$ the binding energy predicted by this method is significantly larger than experiment and for $n = 4$ very much larger than experiment. It is not clear why this method fails for the higher order clusters but it appears to do so.

5. Conclusions

The sequential binding energies of CH_4 ligands to Co^+ occur in pairs: $n = 1$ and $n = 2$ at about 24 ± 1 kcal/mol; $n = 3$ and $n = 4$ at about 6 ± 1 kcal/mol; and $n = 5$ and $n = 6$ at ~2 kcal/mol.

Theory suggests the $n = 1$ and $n = 2$ pair benefit from the ability to minimize Pauli repulsion, favorably induce *s/d* hybridization, and foster C–H bond sigma donation into partially filled orbitals on Co^+.

Theory also suggests the $n = 3$ and $n = 4$ pair are forced to accept much higher levels of Pauli repulsion since they bond at right angles to the $n = 1$ and 2 pair. They also experience a degree of steric hindrance. This leads not only to much lower binding energies but also much longer Co^+–C bond lengths.

The $n = 5$ and $n = 6$ pair are so weakly bound, they could be thought of as beginning the second solvation shell, an interpretation consistent with the ΔS_T^0 for these associations. The probable structure for the $n = 6$ cluster is quasi octahedral with two short Co^+–C bonds ($n = 1$ and 2), two intermediate Co^+–C bonds ($n = 3$ and 4) and two long Co^+–C bonds ($n = 5$ and 6).

Trace amounts of O_2 appear to contaminate the $m/z = 123$ ion leading to an $O_2Co^+(CH_4)_2$ impurity competing with the $Co^+(CH_4)_4$ cluster. Experimental protocols were established to eliminate the effects on the binding energies reported here. It is speculated that the $O_2Co^+(CH_4)_2$ impurity is responsible for an apparently large binding energy observed for the fourth CH_4 ligand by Haynes et al. using the guided ion beam method.

Acknowledgements

The support of the National Science Foundation under grant no. CHE-9729146 is gratefully acknowledged.

References

[1] B.A. Arndsten, R.G. Bergman, T.A. Mobley, T.H. Peterson, Acc. Chem. Res. 28 (1995) 154.
[2] R.H. Crabtree, Chem. Rev. 85 (1985) 245.
[3] J.C. Weisshaar, Acc. Chem. Res. 26 (1993) 213.
[4] See, for example, Organometallic Ion Chemistry, B.S. Freiser (Ed), Kluwer Academic, Dordrecht, The Netherlands, 1996.
[5] See, for example, R. Tonkyn, M. Ronan, J.C. Weisshaar, J. Phys. Chem. 92 (1988) 92.
[6] P. van Koppen, J. Brodbelt-Lustig, M.T. Bowers, D. Dearden, J.L. Beauchamp, E.R. Fisher, P.B. Armentrout, J. Am. Chem. Soc. 112 (1990) 5663; 115 (1991) 2359.
[7] K.M. Ervin, P.B. Armentrout, J. Chem. Phys. 166 (1985) 83;

R.H. Schultz, P.B. Armentrout, Int. J. Mass Spectrom. Ion Processes 107 (1991) 29.
[8] P.R. Kemper, J. Bushnell, G. von Helden, M.T. Bowers, J. Phys. Chem. 97 (1993) 52; J.E. Bushnell, P.R. Kemper, M.T. Bowers, ibid. 98 (1994) 2044.
[9] See Table of Bond Energies in [4].
[10] P.A.M. van Koppen, J.E. Bushnell, P.R. Kemper, M.T. Bowers, J. Am. Chem. Soc. 117 (1995) 2098.
[11] P.A.M. van Koppen, J. Perry, P.R. Kemper, J.E. Bushnell, M.T. Bowers, Int. J. Mass Spectrom. 187 (1999) 989.
[12] J.E. Bushnell, P.R. Kemper, P. Maître, M.T. Bowers, J. Am. Chem. Soc. 116 (1994) 9710.
[13] C.J. Carpenter, P.A.M. van Koppen, M.T. Bowers, J. Perry, J. Am. Chem. Soc. 122 (2000) 392.
[14] M.T. Bowers, P.R. Kemper, P.A.M. von Koppen, T. Wyttenbach, C.J. Carpenter, P. Weis, J. Gidden, Energetics of Stable Molecules and Reaction Intermediates, M.E. Hinas da Piedade (Ed.), Kluwer Academic, Dordrecht, The Netherlands, 1999, pp. 235–258.
[15] P.R. Kemper, P. Weis, M.T. Bowers, Chem. Phys. Lett. 293 (1998) 503.
[16] P.R. Kemper, J. Bushnell, P.A.M. van Koppen, M.T. Bowers, J. Phys. Chem. 97 (1993) 1810.
[17] C.L. Haynes, P.B. Armentrout, J.K. Perry, W.A. Goddard III, J. Phys. Chem. 99 (1995) 6340.
[18] J.K. Perry, G. Ohanessian, W.A. Goddard III, J. Phys. Chem. 97 (1993) 5238.
[19] J.E. Bushnell, P.R. Kemper, M.T. Bowers, J. Phys. Chem. 97 (1993) 11628; P.R. Kemper, J.E. Bushnell, P. Maître, M.T. Bowers, Chem. Phys. Lett. 242 (1995) 244.
[20] P.R. Kemper, P. Weis, M.T. Bowers, P. Maître, J. Am. Chem. Soc. 120 (1998) 13494.
[21] P.R. Kemper, P. Weis, M.T. Bowers, Int. J. Mass Spectrom. Ion Processes 160 (1997) 17.
[22] P.R. Kemper, M.T. Bowers, J. Am. Soc. Mass Spectrom. 1 (1990) 197.
[23] Q. Zhang, P.R. Kemper, M.T. Bowers, to be published.
[24] P.J. Stephens, F.J. Devlin, C.F. Chabalowski, M.J. Frisch, J. Phys. Chem. 98 (1994) 11623.
[25] A. Becke, J. Chem. Phys. 98 (1993) 5648.
[26] GAUSSIAN98, M.J. Frisch, G.W. Trucks, H.B. Schlegel, G.E. Scuseria, M.A. Robb, J.R. Cheeseman, V.G. Zakrzewski, J.A. Montgomery Jr., R.E. Stratmann, J.C. Burant, S. Dapprich, J.M. Millam, A.D. Daniels, K.N. Kudin, M.C. Strain, O. Farkas, J. Tomasi, V. Barone, M. Cossi, R. Cammi, B. Mennucci, C. Pomelli, C. Adamo, S. Clifford, J. Ochterski, G.A. Petersson, P.Y. Ayala, Q. Cui, K. Morokuma, D.K. Malick, A.D. Rabuck, K. Raghavachari, J.B. Foresman, J. Cioslowski, J.V. Ortiz, A.G. Baboul, B.B. Stefanov, G. Liu, A. Liashenko, P. Piskorz, I. Komaromi, R. Gomperts, R.L. Martin, D.J. Fox, T. Keith, M.A. Al-Laham, C.Y. Peng, A. Nanayakkara, C. Gonzalez, M. Challacombe, P.M.W. Gill, B. Johnson, W. Chen, M.W. Wong, J.L. Andres, C. Gonzalez, M. Head-Gordon, E.S. Replogle, J.A. Pople, Gaussian, Inc., Pittsburgh, PA, 1998.
[27] N. Godbout, D.R. Salahub, J. Andzelm, E. Wimmer, Can. J. Chem. 70 (1992) 560.
[28] A.J.H. Wachters, J. Chem. Phys. 52 (1970) 1033.
[29] A.E. Reed, L.A. Curtis, F. Weinhold, Chem. Rev. 88 (1988) 899.
[30] We used the program in GAUSSIAN98 in [26].
[31] (a) C.W. Bauschlicher, H. Partridge, S.R. Langhoff, J. Chem. Phys. 91 (1989) 4733; (b) H. Partridge, C.W. Bauschlicher, S.R. Langhoff, J. Phys. Chem. 96 (1992) 5350; (c) C.W. Bauschlicher, H. Partridge, S.R. Langhoff, Chem. Phys. Lett. 165 (1990) 272.
[32] J.E. Bushnell, P. Maître, P.R. Kemper, M.T. Bowers, J. Chem. Phys. 106 (1997) 10153.